

# The role of flexural coupling in heat dissipation from a two-dimensional layered material to its hexagonal boron nitride substrate

Zhun-Yong Ong,\* Gang Zhang, and Yong-Wei Zhang

*Institute of High Performance Computing, A\*STAR, Singapore 138632, Singapore*

(Dated: April 19, 2021)

Understanding the limits of phononic heat dissipation from a two-dimensional layered material (2DLM) to its hexagonal boron nitride (h-BN) substrate and how it varies with the structure of the 2DLM is important for the design and thermal management of h-BN-supported nanoelectronic devices. We formulate an elasticity-based theory to model the phonon-mediated heat dissipation between a 2DLM and its h-BN substrate. By treating the h-BN substrate as a semi-infinite stack of harmonically coupled thin plates, we obtain semi-analytical expressions for the thermal boundary conductance (TBC) and interfacial phonon transmission spectrum. We evaluate the temperature-dependent TBC of the  $N$ -layer 2DLM (graphene or MoS<sub>2</sub>) on different common substrates (h-BN vs. a-SiO<sub>2</sub>) at different values of  $N$ . The results suggest that h-BN is substantially more effective for heat dissipation from MoS<sub>2</sub> than a-SiO<sub>2</sub> especially at large  $N$ . To understand the limitations of our stack model, we also compare its predictions in the  $N = \infty$  limit to those of the more exact Atomistic Green's Function model for the graphite-BN and molybdenite-BN interfaces. Our stack model provides clear insights into the key role of the flexural modes in the TBC and how the anisotropic elastic properties of h-BN affect heat dissipation.

## I. INTRODUCTION

Bulk hexagonal boron nitride (h-BN) is widely used as a substrate and encapsulating material for nanoscale devices based on two-dimensional (2D) layered materials [1, 2] because its atomically flat surface, which is free of dangling bonds and charged impurities, enhances device performance by reducing the mechanical perturbation to the active 2D layered material (e.g. graphene or MoS<sub>2</sub>), unlike conventional insulating substrates, such as amorphous SiO<sub>2</sub> (a-SiO<sub>2</sub>) and Al<sub>2</sub>O<sub>3</sub>, which have corrugated surfaces [3–6]. In addition, the h-BN has other material properties (e.g. electrically insulating, chemical stability, mechanical flexibility and high in-plane thermal conductivity [7–10]) which are highly advantageous for the development of 2D nanoelectronics.

In spite of its many desirable material properties, a potential obstacle to the integration of h-BN into 2D nanoelectronic devices is the thermal resistance of its interface with the two-dimensional layered material (2DLM), which can lead to a heat dissipation bottleneck and limit device performance if the Joule heat is not removed efficiently [11]. In an active 2DLM-based device on a h-BN substrate, the generated Joule heat is transferred from the 2DLM to the h-BN across their interface through the relatively weak van der Waals (vdW) forces coupling of the thermal motion of the atoms in the 2DLM and on the substrate surface [12, 13]. The rate at which heat is dissipated across this interface varies with its thermal boundary conductance (TBC) and depends on the strength of the vdW forces and the elastic properties of the 2DLM and h-BN.

In bulk h-BN, the stacking of the individual h-BN layers, which is responsible for its characteristic surface flatness, also gives rise to its anisotropic elastic properties

and, in a 2D device, affects how the vdW forces dissipate energy across the interface between the 2DLM and its h-BN substrate. Given the potential of h-BN for 2D device applications, physical insights into how a 2DLM dissipates heat through its planar interface with h-BN are critical for the development of thermally efficient nanoelectronics [11, 12] as well as for understanding the theoretical limits of substrate-directed heat dissipation. Although atomistic thermal transport simulations can play an important role in obtaining these insights [14], they suffer from finite-size effects and it is more challenging to connect their results to the elastic properties of the materials. Hence, it is useful to develop theoretical models that use simple elastic parameters (e.g. bending rigidity and interlayer force constants) as inputs because they can be modified easily to predict how the choice of substrate material and device structure (e.g. dielectric encapsulation and thickness of the 2DLM) affects heat dissipation or isolation [15]. Such models have been developed for isotropic elastic solid substrates, such as a-SiO<sub>2</sub> [16, 17], to understand the effects of encapsulation [17] and the thickness of the 2DLM [18] on the TBC but they cannot be applied to h-BN at present because of its highly anisotropic elastic properties.

To understand how the elastic properties of the substrate affect heat dissipation, let us recall the formula for the phonon TBC which we can write in the Landauer form [17] as

$$G_{\text{ph}} = \int \frac{d\omega}{2\pi} \hbar\omega \frac{dN(\omega, T)}{dT} \xi(\omega), \quad (1)$$

where  $N(\omega, T)$  denotes the Bose-Einstein distribution function,

$$\xi(\omega) = \int_{q < q_c} \frac{d^2q}{(2\pi)^2} \Xi(\mathbf{q}, \omega) \quad (2)$$

is the total areal transmission function at frequency  $\omega$ , and  $q_c$  is the cutoff transverse wave vector of the 2DLM such that  $\pi q_c^2$  is the area of its Brillouin zone. In Eq. (2),  $\xi(\omega)$  can be interpreted as the spectral window for phonon transmission and is obtained by summing the modal transmission function  $\Xi(\mathbf{q}, \omega)$  over the 2D transverse wave vector  $\mathbf{q}$ . The expression for  $\Xi(\mathbf{q}, \omega)$  is [17]

$$\Xi(\mathbf{q}, \omega) = \frac{4K^2 \text{Im}D_{\text{sub}}(\mathbf{q}, \omega) \text{Im}D_{2\text{D}}(\mathbf{q}, \omega)}{[1 - K[D_{\text{sub}}(\mathbf{q}, \omega) + D_{2\text{D}}(\mathbf{q}, \omega)]]^2}, \quad (3)$$

where  $K$  is the areal spring constant at the 2DLM-substrate interface,  $D_{\text{sub}}(\mathbf{q}, \omega)$  is the Green's function for the substrate surface displacement which describes how it responds to an applied normal force, and  $D_{2\text{D}}(\mathbf{q}, \omega)$  is the Green's function for the flexural motion of the 2DLM which can be single or multilayered. Equation (3) satisfies the condition  $0 \leq \Xi(\mathbf{q}, \omega) < 1$  [17] and can be interpreted as the fraction of energy transmitted across the 2DLM-substrate interface at  $\mathbf{q}$  and  $\omega$ . It also assumes that the energy transfer at the interface is due entirely to the harmonic coupling between the 2DLM and its substrate, with the anharmonicity of the interfacial bonds playing an insignificant role. In this model [17], we assume that the  $D_{\text{sub}}(\mathbf{q}, \omega)$  and  $D_{2\text{D}}(\mathbf{q}, \omega)$  are isotropic with respect to  $\mathbf{q}$ , depending only on its magnitude  $q = |\mathbf{q}|$  and  $\omega$ . The analytical expression for the  $D_{\text{sub}}(\mathbf{q}, \omega)$  of an *isotropic* elastic solid substrate, which depends on the speed of sound and mass density of the solid, is derived in Ref. [19] and has been used with Eq. (1) to estimate the TBC between 2DLMs (e.g. graphene and MoS<sub>2</sub>) and a-SiO<sub>2</sub> [16–18]. However, for a layered substrate such as h-BN, our ability to calculate the TBC of the 2DLM-substrate interface is limited by the lack of an expression for  $D_{\text{sub}}(\mathbf{q}, \omega)$  that describes its anisotropic elastic character and layered geometry.

In this paper, we address this problem by formulating an anisotropic model of the h-BN substrate that is based on linear elasticity theory and treats the h-BN lattice as a semi-infinite stack of harmonically coupled thin plates. Our approach builds on the theoretical concepts developed in Refs. [17, 18]. Although our ‘stack model’ is specifically used to treat h-BN in this paper, the theory can be easily extended to other 2D layered analogs of bulk h-BN (e.g. graphite) and may also be useful for understanding the dynamics of breathing modes in 2DLMs [20, 21] as well as for estimating the substrate-induced changes in the properties of a h-BN-supported 2DLM using many-body techniques [22]. We solve our stack model to derive an analytical expression for  $D_{\text{sub}}(\mathbf{q}, \omega)$  which is verified numerically. We then apply Eq. (1) to compute the TBC for different 2DLMs (graphene and MoS<sub>2</sub>) and substrates (a-SiO<sub>2</sub> and h-BN). We analyze how the substrate affects the dependence of the TBC on the temperature and number of layers in the 2DLM. We also compare the predictions of our stack model to those of the Atomistic Green's Function (AGF)

method [14], which is computationally more expensive and atomistically more detailed, to uncover the role of the flexural phonons in interfacial thermal transport. Finally, we examine how the TBC varies with the interlayer spring constant strength from the weak (van der Waals) to the strong coupling limit. We note here that the model described in this paper can be extended to 2DLMs with defects, such as grain boundaries, by modifying the bending rigidity and flexural phonon lifetimes which are reduced by defect scattering. [23]

## II. METHODOLOGY

### A. Theory of h-BN

#### 1. Stack model of harmonically coupled thin plates

The key idea in our derivation of  $D_{\text{sub}}$  is that the h-BN lattice is treated as a continuum in the in-plane  $x$  and  $y$  directions and as a discrete system in the cross-plane  $z$  direction in order to capture the anisotropic character of the lattice. As in Refs. [17] and [18], we only consider the flexural motion and ignore the in-plane polarized degrees of freedom in the individual layers for the sake of simplicity. We treat the h-BN substrate as a semi-infinite stack of sheets, indexed  $n = 1, \dots, \infty$  where layer 1 is at the top surface, as shown in Fig. 1 with each sheet is modeled as a thin plate. We assume that adjacent sheets, separated by an interlayer distance of  $a$ , are coupled via a harmonic force. The stacking order of the individual h-BN layers is ignored in our model because of its continuum nature.

Our objective is to determine how the flexural displacement of the top layer  $u_1(\mathbf{r}, t)$ , where  $\mathbf{r} = (x, y)$  and  $t$  represent respectively the in-plane position and time, oscillates when an external harmonic normal force  $\sigma_{\text{ext}}(\mathbf{r}, t)$  is applied on layer 1 in the  $z$  direction. In other words, we want to find the frequency response function  $D_{11}(\mathbf{q}, \omega)$ , which is the  $D_{\text{sub}}(\mathbf{q}, \omega)$  in Eq. (3), in the linear relationship

$$\tilde{u}_1(\mathbf{q}, \omega) = -D_{11}(\mathbf{q}, \omega) \tilde{\sigma}_{\text{ext}}(\mathbf{q}, \omega) \quad (4)$$

where  $\tilde{u}_1(\mathbf{q}, \omega) = \frac{1}{(2\pi)^3} \int d\mathbf{r} \int dt u_1(\mathbf{r}, t) e^{-i(\mathbf{q}\cdot\mathbf{r} - \omega t)}$  is the Fourier transform of the position and time-dependent flexural displacement of layer 1  $u_1(\mathbf{r}, t)$ , and  $\tilde{\sigma}_{\text{ext}}(\mathbf{q}, \omega) = \frac{1}{(2\pi)^3} \int d\mathbf{r} \int dt \sigma_{\text{ext}}(\mathbf{r}, t) e^{-i(\mathbf{q}\cdot\mathbf{r} - \omega t)}$  is the Fourier transform of the position and time-dependent applied external normal force  $\sigma_{\text{ext}}(\mathbf{r}, t)$ . Finding this response of the top layer is however complicated by the collectively coupled motion of the layers in the semi-infinite stack. In the rest of the subsection, we show how an analytical expression for  $D_{11}(\mathbf{q}, \omega)$  can be obtained by exploiting the matrix structure of the coupled equations of motion. To avoid confusion with the symbol for angular frequency  $\omega$  in the rest of the paper, we use the symbol  $u$  instead of  $w$  as

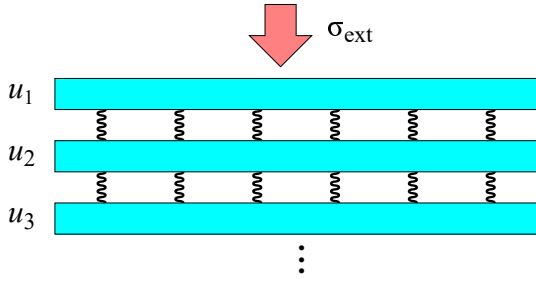


Figure 1. Schematic of the semi-infinite stack model for h-BN. The external normal force  $\sigma_{\text{ext}}$  is applied to layer 1, which is at the top of the stack, while the flexural motion of the individual layers is coupled harmonically via spring-like harmonic forces as indicated by the wavy lines.

per the convention in linear elasticity theory to represent displacement in the out-of-plane  $z$  direction.

We begin our derivation with the equations of motion for the individual layers in h-BN. The equation of motion for the top layer (layer 1) is

$$\rho \frac{\partial^2 u_1}{\partial t^2} = -\kappa \nabla^2 \nabla^2 u_1 - g(u_1 - u_2) + \sigma_{\text{ext}}, \quad (5)$$

where  $\nabla^2 = \frac{\partial^2}{\partial x^2} + \frac{\partial^2}{\partial y^2}$  is the in-plane Laplace operator,  $\rho$  is the areal mass density,  $u_n = u_n(\mathbf{r}, t)$  is the position and time-dependent flexural displacement of layer  $n$  ( $n = 1, \dots, \infty$ ) from its equilibrium position,  $\kappa$  is the sheet bending rigidity, and  $g$  is the interlayer areal spring constant. The second term on the righthand side (RHS) of Eq. (5) represents the harmonic coupling between layers 1 and 2. If we set  $g = 0$  and  $\sigma_{\text{ext}} = 0$ , we recover the classic Kirchhoff-Love equation [24] ( $\rho \frac{\partial^2 u_1}{\partial t^2} = -\kappa \nabla^2 \nabla^2 u_1$ ) for the flexural motion of a thin plate [16, 17]. The equation of motion for the remaining subsurface layers ( $n \geq 2$ ) in general can be similarly written as

$$\rho \frac{\partial^2 u_n}{\partial t^2} = -\kappa \nabla^2 \nabla^2 u_n - g(u_n - u_{n-1}) - g(u_n - u_{n+1}), \quad (6)$$

where the second and third terms on the RHS of Eq. (6) represent the harmonic coupling to its top and bottom neighboring layers, respectively. If we define the Fourier transform of a function  $f(\mathbf{r}, t)$  as  $\tilde{f}(\mathbf{q}, \omega) = \frac{1}{(2\pi)^3} \int d\mathbf{r} \int dt f(\mathbf{r}, t) e^{-i(\mathbf{q}\cdot\mathbf{r} - \omega t)}$ , then the Fourier transform of Eq. (5) yields the algebraic equation

$$-\rho\omega^2 \tilde{u}_1 = -\kappa q^4 \tilde{u}_1 - g(\tilde{u}_1 - \tilde{u}_2) + \tilde{\sigma}_{\text{ext}} \quad (7)$$

while Eq. (6) yields

$$-\rho\omega^2 \tilde{u}_n = -\kappa q^4 \tilde{u}_n - g(\tilde{u}_n - \tilde{u}_{n-1}) - g(\tilde{u}_n - \tilde{u}_{n+1}). \quad (8)$$

We note here that when h-BN is strained, its flexural phonon dispersion becomes linear in the long wavelength limit as a result of stiffening of the flexural modes [25] like in graphene [26] and a term proportional to  $q^2$  should

be added to the RHS of Eqs. (7) and (8). However, this is unlikely to affect the TBC between the 2DLM and h-BN significantly because, as we shall see later, the low-frequency portion of the transmission spectrum is not significant.

Proceeding further with our analysis, we combine Eqs. (7) and (8) to obtain the matrix equation

$$-z(\mathbf{q}, \omega) \tilde{\mathbf{u}}(\mathbf{q}, \omega) = -\mathbf{H} \tilde{\mathbf{u}}(\mathbf{q}, \omega) + \tilde{\boldsymbol{\sigma}}(\mathbf{q}, \omega), \quad (9)$$

where  $z(\mathbf{q}, \omega) = \rho\omega^2 - \kappa q^4$  represents the inverse of the response function of a decoupled h-BN layer,  $\tilde{\mathbf{u}}(\mathbf{q}, \omega) = (\tilde{u}_1 \ \tilde{u}_2 \ \tilde{u}_3 \ \dots)^T$ ,  $\tilde{\boldsymbol{\sigma}}(\mathbf{q}, \omega) = (\tilde{\sigma}_{\text{ext}} \ 0 \ 0 \ \dots)^T$ , and

$$\mathbf{H} = \begin{pmatrix} g & -g & 0 & \dots \\ -g & 2g & -g & \dots \\ 0 & -g & 2g & \ddots \\ \vdots & \vdots & \ddots & \ddots \end{pmatrix}$$

is a matrix describing the interlayer coupling. We can rewrite Eq. (9) as

$$\tilde{\mathbf{u}}(\mathbf{q}, \omega) = -\mathbf{D}(\mathbf{q}, \omega) \tilde{\boldsymbol{\sigma}}(\mathbf{q}, \omega) \quad (10)$$

where

$$\mathbf{D}(\mathbf{q}, \omega) = \begin{pmatrix} D_{11}(\mathbf{q}, \omega) & D_{12}(\mathbf{q}, \omega) & D_{31}(\mathbf{q}, \omega) & \dots \\ D_{21}(\mathbf{q}, \omega) & D_{22}(\mathbf{q}, \omega) & D_{32}(\mathbf{q}, \omega) & \dots \\ D_{31}(\mathbf{q}, \omega) & D_{32}(\mathbf{q}, \omega) & D_{33}(\mathbf{q}, \omega) & \ddots \\ \vdots & \vdots & \ddots & \ddots \end{pmatrix} \quad (11)$$

is the response function of the semi-infinite stack, i.e.,  $\mathbf{D}(\mathbf{q}, \omega) = [z(\mathbf{q}, \omega)\mathbf{I} - \mathbf{H}]^{-1}$ , and  $\mathbf{I}$  is the identity matrix. Most of the matrix elements of  $\mathbf{D}(\mathbf{q}, \omega)$  are not relevant for our problem since we only need  $D_{11}(\mathbf{q}, \omega)$ , the first diagonal matrix element in Eq. (11), to determine how  $\tilde{u}_1(\mathbf{q}, \omega)$  responds to  $\tilde{\sigma}_{\text{ext}}(\mathbf{q}, \omega)$  because Eq. (10) implies that  $\tilde{u}_1(\mathbf{q}, \omega) = -D_{11}(\mathbf{q}, \omega) \tilde{\sigma}_{\text{ext}}(\mathbf{q}, \omega)$ . We note that because the matrices and column vectors in Eq. (9) are infinitely large, it is impossible to determine  $D_{11}(\mathbf{q}, \omega)$  from direct matrix inversion. Instead, an alternative approach is needed.

## 2. Analytical expression for $D_{11}(\mathbf{q}, \omega)$

As shown earlier in Ref. [17],  $D_{11}(\mathbf{q}, \omega)$  must satisfy the relationship

$$D_{11}(\mathbf{q}, \omega) = [z(\mathbf{q}, \omega) - P(\mathbf{q}, \omega)]^{-1} \quad (12)$$

where  $P(\mathbf{q}, \omega) = g[1 - gD_{22}^{(0)}(\mathbf{q}, \omega)]^{-1}$  is the ‘self-energy’ term representing the effect of the subsurface layers ( $n \geq 2$ ) coupling to the top layer ( $n = 1$ ), and  $D_{22}^{(0)}$

is the second diagonal matrix element in  $\mathbf{D}_0(\mathbf{q}, \omega) = [z(\mathbf{q}, \omega)\mathbf{I} - \mathbf{H}_0]^{-1}$  for

$$\mathbf{H}_0 = \begin{pmatrix} 0 & 0 & 0 & \dots \\ 0 & g & -g & \dots \\ 0 & -g & 2g & \ddots \\ \vdots & \vdots & \ddots & \ddots \end{pmatrix}.$$

Physically,  $D_{22}^{(0)}$  represents the response of the semi-infinite stack ( $n = 2, 3, \dots$ ) in layer 2 when layer 1 is decoupled from the layer 2. This decoupling effectively turns layer 2 into the surface layer of a semi-infinite stack and we thus deduce that  $D_{22}^{(0)}(\mathbf{q}, \omega) = D_{11}(\mathbf{q}, \omega)$ . Hence, we obtain for Eq. (12) the expression

$$D_{11}(\mathbf{q}, \omega) = \left[ z(\mathbf{q}, \omega) - \frac{g}{1 - gD_{11}(\mathbf{q}, \omega)} \right]^{-1}, \quad (13)$$

which we rewrite as an equation quadratic in  $D_{11}$ , i.e.,

$$D_{11}(\mathbf{q}, \omega)[1 - gD_{11}(\mathbf{q}, \omega)] = z(\mathbf{q}, \omega)^{-1}. \quad (14)$$

The solution to Eq. (14) is

$$D_{11}^{\pm}(\mathbf{q}, \omega) = \frac{2}{z(\mathbf{q}, \omega) \pm \sqrt{z(\mathbf{q}, \omega)^2 - 4z(\mathbf{q}, \omega)g}}. \quad (15)$$

However,  $D_{11}^+(\mathbf{q}, \omega)$  and  $D_{11}^-(\mathbf{q}, \omega)$  are not the solutions to Eq. (13) for  $z \in \mathbb{R}$  because they do not satisfy the constraints on their asymptotic behavior imposed by Eq. (14). We also observe that  $D_{11}^{\pm}(\mathbf{q}, \omega)$  has a singularity at  $z = 0$ , where the denominator in Eq. (15) is zero, corresponding to the surface states of the semi-infinite stack model. Thus, we have to treat  $D_{11}(\mathbf{q}, \omega)$  differently for  $z > 0$  and  $z < 0$ . For  $z \rightarrow \pm\infty$ , Eq. (14) has to scale asymptotically as  $\lim_{z \rightarrow \pm\infty} D_{11}(\mathbf{q}, \omega) = z(\mathbf{q}, \omega)^{-1}$ , a condition which can only be satisfied if we choose  $D_{11}(\mathbf{q}, \omega) = D_{11}^-(\mathbf{q}, \omega)$  for  $z < 0$  and  $D_{11}(\mathbf{q}, \omega) = D_{11}^+(\mathbf{q}, \omega)$  for  $z > 0$ . Therefore, the surface response function is

$$D_{\text{sub}}(\mathbf{q}, \omega) = \Theta(z)D_{11}^+(\mathbf{q}, \omega) + \Theta(-z)D_{11}^-(\mathbf{q}, \omega), \quad (16)$$

where  $\Theta(\dots)$  is the Heaviside function.

If  $0 < z(\mathbf{q}, \omega) \leq 4g$ , then  $D_{\text{sub}}(\mathbf{q}, \omega)$  has an imaginary component and can be written as

$$D_{\text{sub}}(\mathbf{q}, \omega) = \frac{2}{z(\mathbf{q}, \omega) + i\sqrt{4z(\mathbf{q}, \omega)g - z(\mathbf{q}, \omega)^2}}, \quad (17)$$

where  $z(\mathbf{q}, \omega) = \rho\omega^2 - \kappa q^4$ , to give us

$$\text{Re}D_{\text{sub}}(\mathbf{q}, \omega) = \frac{1}{2g} \quad (18a)$$

and

$$\text{Im}D_{\text{sub}}(\mathbf{q}, \omega) = -\frac{\sqrt{4z(\mathbf{q}, \omega)g - z(\mathbf{q}, \omega)^2}}{2z(\mathbf{q}, \omega)g}. \quad (18b)$$

Outside of the range  $0 < z(\mathbf{q}, \omega) \leq 4g$ , the expression for  $D_{\text{sub}}(\mathbf{q}, \omega)$  in Eq. (16) has no imaginary component for  $z(\mathbf{q}, \omega) < 0$  or  $z(\mathbf{q}, \omega) > 4g$ . The finiteness of  $\text{Im}D_{\text{sub}}(\mathbf{q}, \omega)$  when  $0 < z(\mathbf{q}, \omega) \leq 4g$  is a result of the existence of bulk flexural modes which satisfy the dispersion relation

$$\omega(q, k) = \sqrt{\frac{\kappa q^4}{\rho} + \frac{4g}{\rho} \sin^2\left(\frac{ka}{2}\right)}, \quad (19)$$

where  $k$  is the wave vector associated with periodicity in the cross-plane ( $z$ ) direction. Equation (19), which can be derived from the phonon dispersion of the one-dimensional monoatomic lattice chain [27], also implies that  $\omega \leq \sqrt{\frac{1}{\rho}(\kappa q_c^4 + 4g)}$ .

Physically, the nonzero  $\text{Im}D_{\text{sub}}(\mathbf{q}, \omega)$  implies that the surface displacement from the applied external force  $\tilde{\sigma}_{\text{ext}}(\mathbf{q}, \omega)$  dissipates into the h-BN substrate as bulk flexural waves. This is the mechanism for interfacial heat transfer between the 2DLM and h-BN since  $\tilde{\sigma}_{\text{ext}}(\mathbf{q}, \omega)$  is generated from the harmonic forces at the interface and the energy from this interaction is dissipated into the substrate bulk.

### 3. Numerical verification of $D_{\text{sub}}(\mathbf{q}, \omega)$ formula

To verify that Eq. (16) is correct numerically, we make use of Eq. (12) to define the  $n$ -th order approximation to  $D_{\text{sub}}(\mathbf{q}, \omega)$  as

$$D_{\text{sub}}^{(n)}(\mathbf{q}, \omega) = \left[ z(\mathbf{q}, \omega) - \frac{g}{1 - gD_{\text{sub}}^{(n-1)}(\mathbf{q}, \omega)} \right]^{-1} \quad (20)$$

for  $n \geq 1$  and  $D_{\text{sub}}^{(0)}(\mathbf{q}, \omega) = z(\mathbf{q}, \omega)^{-1}$ . Physically,  $D_{\text{sub}}^{(n)}(\mathbf{q}, \omega)$  can be interpreted as the surface response function for a finite stack with  $n + 1$  layers [18]. We expect Eq. (20) to converge to Eq. (16) as we iterate it over  $n$ , i.e.,  $\lim_{n \rightarrow \infty} D_{\text{sub}}^{(n)} = D_{\text{sub}}$ .

In our numerical tests to check if  $\lim_{n \rightarrow \infty} D_{\text{sub}}^{(n)} = D_{\text{sub}}$ , we treat  $D_{\text{sub}}$  and  $D_{\text{sub}}^{(n)}$  as functions of  $z$  which can be either positive or negative. We compute  $D_{\text{sub}}$  and  $D_{\text{sub}}^{(n)}$  for  $-3g \leq z \leq 7g$ , with the  $z = 0$  point excluded. To ensure convergence in the computation of  $D_{\text{sub}}^{(n)}$  when  $0 < z \leq 4g$ , we make the substitution  $z \rightarrow z + i\eta(z)$ , where  $\eta(z) = 0.01z$ , in Eq. (20). We find that convergence is easily achieved at relatively small values of  $n$  ( $n \sim 20$ ) for  $z < 0$  and  $z > 4g$  where  $\text{Im}D_{\text{sub}}(\mathbf{q}, \omega) = 0$ . However, in the  $0 < z \leq 4g$  range where  $\text{Im}D_{\text{sub}} \neq 0$ , much higher values of  $n$  ( $n \gtrsim 1500$ ) are needed for convergence especially at smaller  $z$  values. Figure 2 shows  $D_{\text{sub}}^{(n)}$  at  $n = 2000$  and  $D_{\text{sub}}$  for comparison. We observe excellent agreement between the approximate and analytical results from Eqs. (20) and (16), respectively, verifying that formula for  $D_{\text{sub}}(\mathbf{q}, \omega)$  in Eq. (16) is correct.

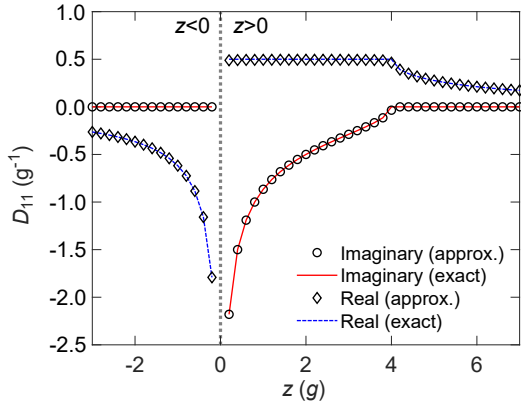


Figure 2. Plot of  $\text{Re}D_{\text{sub}}$  (dashed blue line),  $\text{Im}D_{\text{sub}}$  (solid red line),  $\text{Re}D_{\text{sub}}^{(n)}$  (diamond symbols), and  $\text{Im}D_{\text{sub}}^{(n)}$  (circle symbols) from Eqs. (16) and (20), respectively, for  $-3g \leq z \leq 7g$  at  $n = 2000$ . The  $z = 0$  point is excluded.

### B. Elasticity-based models of multilayer 2D layered materials and amorphous $\text{SiO}_2$

In order to apply Eq. (3) for an  $N$ -layer 2DLM, we also need the expression for  $D_{2\text{D}}(\mathbf{q}, \omega)$  for different values of  $N$ . Although the formulas are given in Ref. [18], we provide them here for the sake of completeness. The expression for the  $D_{2\text{D}}(\mathbf{q}, \omega)$  of a 1-layer 2DLM is [17]

$$D_{2\text{D},1}(\mathbf{q}, \omega) = \frac{1}{\rho\omega^2 + i\rho\gamma(\omega, T)\omega - \kappa q^4} \quad (21)$$

where  $\rho$  is the areal mass density,  $\gamma(\omega)$  is the frequency-dependent damping function, and  $\kappa$  is the bending rigidity, for a single-layer 2DLM. At temperature  $T$ , we can approximate the damping function [17] as  $\gamma(\omega, T) = \frac{\omega T}{\alpha T_{\text{RT}}}$ , where  $T_{\text{RT}}$  is the room temperature and  $\alpha$  is the ratio of the flexural mode frequency to its inverse lifetime at  $T = T_{\text{RT}}$ . Phenomenologically, the frequency-dependent damping function  $\gamma(\omega, T)$  is proportional to  $\omega$  [28] and represents the coupling and exchange of energy between the flexural phonons and other intrinsic degrees of freedom in the 2DLM. In the language of many-body physics,  $\gamma(\omega, T)$  corresponds to the self-energy from the interaction (e.g. anharmonic phonon-phonon and electron-phonon coupling) of the flexural phonons with other intrinsic degrees of freedom and plays an analogous role to the Büttiker probe self-energy terms used in Ref. [29]. The temperature dependence of  $\gamma(\omega, T)$  means that  $D_{2\text{D}}(\mathbf{q}, \omega)$  and hence the total transmission function  $\xi(\omega)$  in Eq. (2) are temperature-dependent. In 2DLM's with defects,  $\gamma(\omega, T)$  can also include the effects of defect scattering [23] which increases the damping rate and leads to higher dissipation rates. For an  $N$ -layer 2DLM ( $N > 1$ ), the corresponding expression for the flexural

response at the 2DLM-substrate interface is [18]

$$D_{2\text{D},N}(\mathbf{q}, \omega) = \sum_{n=1}^N \frac{f_n}{D_{2\text{D},1}(\mathbf{q}, \omega)^{-1} - z_n} \quad (22)$$

where  $z_n = 4g \sin^2[\frac{(n-1)\pi}{2N}]$ ,  $g$  is the interlayer spring constant,  $f_1 = \frac{1}{N}$ , and  $f_n = \frac{1}{N}[1 + \cos\frac{(n-1)\pi}{N}]$  for  $1 < n \leq N$ . We can estimate  $g$  from the  $\Gamma$ -point interlayer breathing modes and obtain  $g = 10.95 \times 10^{19}$  N/m<sup>3</sup> and  $g = 8.60 \times 10^{19}$  N/m<sup>3</sup> for graphene [18] and MoS<sub>2</sub> [20, 21], respectively. In the  $N \rightarrow \infty$  limit, we recover the expression in Eq. (16), i.e.,

$$\lim_{\gamma \rightarrow 0} D_{2\text{D},\infty}(\mathbf{q}, \omega) = \frac{\Theta(\zeta)}{\zeta + \sqrt{\zeta^2 - 4\zeta g}} + \frac{\Theta(-\zeta)}{\zeta - \sqrt{\zeta^2 - 4\zeta g}} \quad (23)$$

where  $\zeta = \lim_{\gamma \rightarrow 0} D_{2\text{D},1}(\mathbf{q}, \omega)^{-1}$ . To model the interface between an  $N = \infty$  2DLM and its substrate, we set  $\gamma(\omega, T) = 0$  so that  $D_{2\text{D}}(\mathbf{q}, \omega) = \lim_{\gamma \rightarrow 0} D_{2\text{D},\infty}(\mathbf{q}, \omega)$  like in Eq. (23). The dissipative term  $\gamma(\omega, T)$  is eliminated in Eq. (23) because the semi-infinite structure of the  $N = \infty$  2DLM ensures that  $D_{2\text{D}}(\mathbf{q}, \omega)$  is dissipative.

To model the surface Green's function for the h-BN substrate, we use the parameters  $\rho = 7.67 \times 10^{-7}$  kg/m<sup>2</sup>,  $\kappa = 0.86$  eV [30] and  $g = 9.83 \times 10^{19}$  N/m<sup>3</sup> [21] in Eq. (16). We assume the maximum wave vector for h-BN to be  $q_{\text{max}} = 2.7 \times 10^{10}$  m<sup>-1</sup> and use Eq. (19) to set  $\omega_{\text{max}} = \sqrt{\frac{1}{\rho}(\kappa q_{\text{cut}}^4 + 4g)} = 204$  meV as the cutoff frequency above which  $D_{\text{sub}}(\mathbf{q}, \omega) = 0$ . To model the surface Green's function for the a-SiO<sub>2</sub> substrate, we approximate it as an isotropic elastic solid for which its surface Green's function is [16, 17]

$$D_{\text{sub}}(\mathbf{q}, \omega) = \frac{i\omega^2}{\rho_{\text{sub}} c_T^4} \frac{p_L(q, \omega)}{S(q, \omega)} \Theta(\omega_D - \omega) \quad (24)$$

where  $S(q, \omega) = [(\omega/c_T)^2 - 2q^2]^2 + 4q^2 p_T(q, \omega) p_L(q, \omega)$ ,  $p_L(q, \omega) = \lim_{\eta \rightarrow 0^+} \sqrt{(\omega/c_L)^2 - q^2 + i\eta}$ , and  $p_T(q, \omega) = \lim_{\eta \rightarrow 0^+} \sqrt{(\omega/c_T)^2 - q^2 + i\eta}$ , with  $\rho_{\text{sub}}$  and  $c_L$  ( $c_T$ ) denoting the voluminal mass density and the longitudinal (transverse) speed of sound in a-SiO<sub>2</sub>, respectively. We set  $\rho_{\text{sub}} = 2200$  kg/m<sup>3</sup>,  $c_L = 5953$  m/s and  $c_T = 2200$  m/s following Ref. [17]. The longitudinal Debye frequency is  $\omega_D = (6\pi^2 N_{\text{sub}} c_L^3)^{1/3} = 62$  meV where  $N_{\text{sub}} = 6.62 \times 10^{28}$  m<sup>-3</sup> is the number density for a-SiO<sub>2</sub> [31]. To model the harmonic interaction at the interface of the 2DLM and h-BN, we estimate  $K$  from the arithmetic mean of the interlayer spring constant  $g$  for the 2DLM and h-BN.

## III. RESULTS AND DISCUSSION

We compute the TBC numerically, using Eq. (1), for different 2DLMs (graphene and MoS<sub>2</sub>) and substrates (h-BN and a-SiO<sub>2</sub>). We use a-SiO<sub>2</sub> as a contrast in order to

	Graphene	MoS <sub>2</sub>
$\rho$ (kg/m <sup>2</sup> )	$7.63 \times 10^{-7}$	$3.05 \times 10^{-6}$
$\kappa$ (eV)	1.1	9.61
$g$ (10 <sup>19</sup> N/m <sup>3</sup> )	10.95	8.60
$K$ (10 <sup>19</sup> N/m <sup>3</sup> )	12.30 (SiO <sub>2</sub> ) 10.39 (h-BN)	4.94 (SiO <sub>2</sub> ) 9.21 (h-BN)
$\alpha$	100	100
$q_c$ (10 <sup>10</sup> m <sup>-1</sup> )	2.7	2.1

Table I. Simulation parameters for graphene and MoS<sub>2</sub> taken from Refs. [17, 18, 21]. The values of  $K$  for the graphene-SiO<sub>2</sub> and MoS<sub>2</sub>-SiO<sub>2</sub> interface are taken from Ref. [17] while that for the graphene-BN (MoS<sub>2</sub>-BN) interface is estimated from the arithmetic mean of the  $g$  for graphene and h-BN (MoS<sub>2</sub> and h-BN) with  $g = 9.83 \times 10^{19}$  N/m<sup>3</sup> for h-BN [21].

understand the effect of the layered geometry of h-BN on cross-plane substrate-directed heat dissipation from two common 2DLMs. In using Eq. (1), we assume for the sake of simplicity that the temperature dependence of the TBC is due primarily to the temperature-dependent changes in the Bose-Einstein distribution  $N(\omega, T)$  of the phonons and the damping function  $\gamma(\omega, T)$  in Eq. (21).

Here, a few remarks on the effects on anharmonicity are necessary for understanding the limitations of our TBC results. Although it is known that anharmonicity or inelastic phonon scattering [32] can play a role in interfacial thermal transport [32–34], the degree to which it contributes to the TBC remains an open question. Anharmonicity has two attendant effects on interfacial transport: at the interface, anharmonicity enables the decomposition of higher-energy phonons on one side of the interface into two or more lower-energy phonons on the other side [32] while in the bulk of a solid, the anharmonic coupling between the phonons leads to the bulk phonons having a finite lifetime. In this study, we do not study the first effect as a rigorous treatment is beyond the scope and objective of our work. Only the second effect, the finite lifetime of the phonons, is taken into account in our results. It is included indirectly and partially, albeit in a phenomenological fashion, through the damping function  $\gamma(\omega, T)$  in Eq. (21) which estimates the finite phonon lifetime in the 2DLM due to inelastic phonon scattering. Indeed, it is noted in Ref. [17] that for a 2DLM with a *finite* number of layers, the inclusion of a non-zero damping function is needed in order for the thermal resistance of the boundary to be finite, i.e., the flexural modes in the 2DLM cannot dissipate heat to the substrate unless the individual layers have some form of damping.

On the other hand, we make no attempt to model the effects of anharmonicity in the h-BN substrate where anharmonic scattering of the bulk phonons can occur [7]. This is also because the flexural motion of the surface of the h-BN substrate is naturally damped via its harmonic coupling to the subsurface layers in the h-BN, an effect

represented by the ‘self-energy’ term  $P(\mathbf{q}, \omega)$  in Eq. (12). Although it is possible to include a phenomenological damping term in our derivation of  $D_{\text{sub}}$  in Eq. (16), its inclusion would result in the intractability of the derivation and analysis of  $D_{\text{sub}}$ . Moreover, the necessity of including anharmonicity in h-BN remains unclear to us since the theoretical interpretation and analysis of existing experimental data [35, 36] provide no guidance on its inclusion. While discrepancies between purely elastic calculations and experimental measurements of the TBC, such as those for the ZnO/GaN interface [35], suggest that anharmonic effects may play a significant role in the TBC at high temperatures, other results [36] indicate that the contribution to the TBC from inelastic processes can be insignificant even at high temperatures. These differences imply that the importance of interfacial thermal transport may vary with the specific material interface even if anharmonic scattering is important for bulk heat conduction.

### A. Temperature dependence of the TBC

We compare in Fig. 3 the temperature dependence of the TBC  $G_{\text{ph}}$  for the 2DLM-substrate interface with single ( $N = 1$ ) and few-layer ( $N = 2, 5, 10$ ) graphene or MoS<sub>2</sub> as the 2DLM and a-SiO<sub>2</sub> or h-BN as the substrate over the temperature range of  $T = 20$  to 600 K. In addition, we also plot the  $G_{\text{ph}}$  results for the  $N = \infty$  case where the 2DLM is the bulk form of graphene and MoS<sub>2</sub>, corresponding respectively to graphite and molybdenite. In Fig. 3(a), we find that the graphene-substrate TBC increases with  $T$  as well as the number of layers in the 2DLM  $N$  like in Ref. [18], reaching  $G_{\text{ph}} = 135$  MW/K/m<sup>2</sup> (graphite-BN) and  $G_{\text{ph}} = 122$  MW/K/m<sup>2</sup> (graphite-SiO<sub>2</sub>) in the  $N = \infty$  limit at 300 K. This pronounced  $N$ -dependence of the TBC for the graphene-BN interface suggests that the thickness-dependent TBC is a general phenomenon that extends to a wider class of substrates beyond elastically isotropic ones such as SiO<sub>2</sub> [18]. For  $N \leq 10$ , the graphene-SiO<sub>2</sub> TBC is also higher than the graphene-BN TBC, with  $G_{\text{ph}} = 33.5$  MW/K/m<sup>2</sup> and  $G_{\text{ph}} = 19.1$  MW/K/m<sup>2</sup> for the former and latter respectively at  $N = 1$ . This suggests that SiO<sub>2</sub> may be more efficient as a vertical heat sink for few-layer graphene although the significantly lower thermal conductivity of SiO<sub>2</sub> ( $\sim 1.3$  to  $1.5$  W/m/K [37–40]) may make it a sub-optimal choice for overall heat dissipation.

In Fig. 3(b), we find that the MoS<sub>2</sub>-substrate TBC also increases with  $T$  and  $N$ . The MoS<sub>2</sub>-BN TBC is however much larger than the MoS<sub>2</sub>-SiO<sub>2</sub> TBC for all temperatures unlike in graphene. At  $T = 300$  K, we obtain  $G_{\text{ph}} = 5.2$  MW/K/m<sup>2</sup> (MoS<sub>2</sub>-BN) and  $G_{\text{ph}} = 3.1$  MW/K/m<sup>2</sup> (MoS<sub>2</sub>-SiO<sub>2</sub>) for  $N = 1$ , and  $G_{\text{ph}} = 26.7$  MW/K/m<sup>2</sup> (MoS<sub>2</sub>-BN) and  $G_{\text{ph}} = 6.9$  MW/K/m<sup>2</sup> (MoS<sub>2</sub>-SiO<sub>2</sub>) in the  $N = \infty$  limit. Our result of  $G_{\text{ph}} = 26.7$  MW/K/m<sup>2</sup>

for  $N = \infty$  and  $T = 300$  K is comparable to the result of  $20 \text{ MW/K/m}^2$  obtained in Ref. [14] using the Atomistic Green's Function method, which we discuss in Sec. III D. At  $T = 300$  K and  $N = 1$ , the ratio of the graphene-BN TBC to the  $\text{MoS}_2$ -BN TBC is  $16.1/5.2 \sim 3.1$ , in good agreement with the  $\sim 3.1$  ratio obtained in thermometric measurements using Raman spectroscopy [14]. The much larger TBC of the  $\text{MoS}_2$ -BN interface implies that h-BN can be a more effective substrate material than  $\text{SiO}_2$  for heat dissipation from  $\text{MoS}_2$ . A summary comparing the TBC results is shown in Table II. In addition, we also show the layer dependence of the TBC with the a- $\text{SiO}_2$  and h-BN substrates in Figs. 3(c) and (d) for graphene and  $\text{MoS}_2$ , respectively, at  $T = 100, 200$  and  $300$  K.

Could the considerably larger  $G_{\text{ph}}$  for the  $\text{MoS}_2$ -BN interface relative to the  $\text{MoS}_2$ - $\text{SiO}_2$  interface be entirely due to its significantly larger areal spring constant ( $K = 9.21 \times 10^{19} \text{ N/m}^3$  for  $\text{MoS}_2$ -BN vs.  $K = 4.94 \times 10^{19} \text{ N/m}^3$  for  $\text{MoS}_2$ - $\text{SiO}_2$ )? We rescale the  $K$  for the  $\text{MoS}_2$ -BN interface so that it is identical to that for the  $\text{MoS}_2$ - $\text{SiO}_2$  interface (i.e.,  $K = 4.94 \times 10^{19} \text{ N/m}^3$  for the  $\text{MoS}_2$ -BN interface) and repeat the TBC calculations in Fig. 3(b), with the results shown in Fig. 4(a). Although the TBC results for the  $\text{MoS}_2$ -BN interface have decreased significantly as a result of the reduced  $K$ , we find that  $G_{\text{ph}}$  for the  $\text{MoS}_2$ -BN interface is still significantly higher than  $G_{\text{ph}}$  for the  $\text{MoS}_2$ - $\text{SiO}_2$  interface. Like in Fig. 3(b), we also observe the stronger dependence on  $N$  with the  $\text{MoS}_2$ -BN interface compared to the  $\text{MoS}_2$ - $\text{SiO}_2$  interface.

To sharpen our analysis of how the anisotropic layered structure in h-BN affects the TBC, we adjust  $g$ , the interlayer areal spring constant in h-BN, so that the acoustic impedance  $z_0$  in the direction normal to the interface is identical for h-BN and a- $\text{SiO}_2$ . Before the adjustment, we have  $z_0 = \rho_{\text{sub}} c_L = 1.31 \times 10^7 \text{ Pa}\cdot\text{s/m}$  in a- $\text{SiO}_2$  which is higher than the  $z_0 = \sqrt{g\rho} = 8.69 \times 10^6 \text{ Pa}\cdot\text{s/m}$  in h-BN. We increase the  $g$  in h-BN from  $9.83 \times 10^{19} \text{ N/m}^3$  to  $2.24 \times 10^{20} \text{ N/m}^3$  so that its new rescaled  $z_0$  is equal to that of a- $\text{SiO}_2$ . Physically, this amounts to stronger coupling between the h-BN layers and a higher group velocity in the normal direction. Assuming  $K = 4.94 \times 10^{19} \text{ N/m}^3$  for both the  $\text{MoS}_2$ -BN and the  $\text{MoS}_2$ - $\text{SiO}_2$  interfaces, we calculate the  $G_{\text{ph}}$  for  $T = 20$  to  $600$  K and  $N = 1, 2, 5, 10$ , and  $\infty$ , like in Fig. 4(a), with the results shown in Fig. 4(b). Compared to Fig. 4(a), there is a clear decrease in  $G_{\text{ph}}$ , especially for  $N \geq 10$ , for the  $\text{MoS}_2$ -BN interface. Nonetheless, in Fig. 4(b), we still observe that  $G_{\text{ph}}$  for the  $\text{MoS}_2$ -BN interface still has a greater  $N$ -dependence and is significantly higher than  $G_{\text{ph}}$  for the  $\text{MoS}_2$ - $\text{SiO}_2$  interface, further highlighting the possible role of anisotropy in interfacial thermal transport at the  $\text{MoS}_2$ -BN interface.

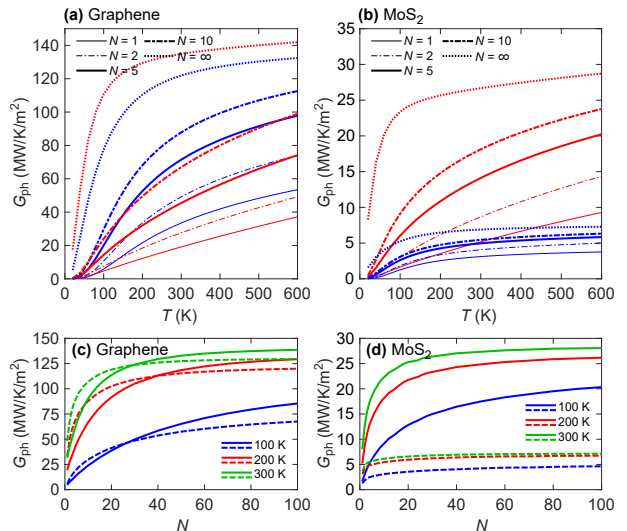


Figure 3. Plot of the TBC  $G_{\text{ph}}$  for single and multi-layer (a) graphene and (b)  $\text{MoS}_2$  with a- $\text{SiO}_2$  (blue lines) or h-BN (red lines) as the substrate over the temperature range of  $T = 20$  to  $600$  K. The TBC is shown for  $N = 1, 2, 5, 10$ , and  $\infty$ . We also plot the layer-dependent TBC for (c) graphene and (d)  $\text{MoS}_2$  with a- $\text{SiO}_2$  (dashed lines) or h-BN (solid lines) as the substrate at  $T = 100, 200$  and  $300$  K.

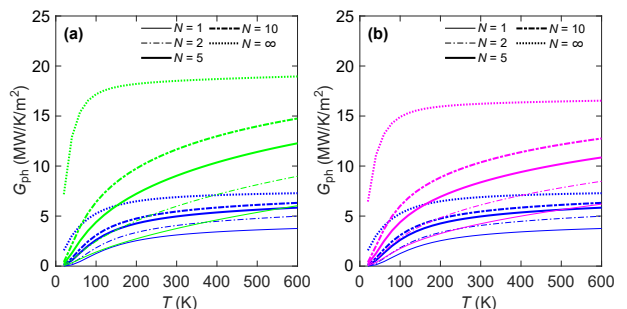


Figure 4. (a) Plot of the TBC  $G_{\text{ph}}$  for single and multi-layer  $\text{MoS}_2$  with a- $\text{SiO}_2$  (blue lines) or h-BN (green lines) as the substrate over the temperature range of  $T = 20$  to  $600$  K, assuming  $K = 4.94 \times 10^{19} \text{ N/m}^3$  for both the  $\text{MoS}_2$ -BN and the  $\text{MoS}_2$ - $\text{SiO}_2$  interfaces. The TBC is shown for  $N = 1, 2, 5, 10$ , and  $\infty$ . (b) Same plot of  $G_{\text{ph}}$  but with  $g = 2.24 \times 10^{20} \text{ N/m}^3$  for the interlayer areal spring constant in h-BN so that its acoustic impedance in the normal direction is identical to that of a- $\text{SiO}_2$ . The  $\text{MoS}_2$ -BN results are indicated with magenta lines. We assume that  $K = 4.94 \times 10^{19} \text{ N/m}^3$  for both the  $\text{MoS}_2$ -BN and the  $\text{MoS}_2$ - $\text{SiO}_2$  interfaces

## B. TBC dependence on the interlayer spring constant in h-BN

Given the sensitivity of the  $\text{MoS}_2$ -BN TBC to the numerical values of  $K$  and  $g$  as seen in Fig. 4, we try to understand more systematically how  $g$  in h-BN affects the TBC by calculating  $G_{\text{ph}}$  for  $N$ -layer graphene and  $\text{MoS}_2$  at different  $g$  values. We set a natural scale for  $g$

Interface	TBC (MW/K/m <sup>2</sup> )		
	Stack model	AGF	Experiment
Graphene-BN ( $N = 1$ )	19.1	–	52.2 [14], 7.6 [41], 10 [42]
MoS <sub>2</sub> -BN ( $N = 1$ )	5.2	–	17.0 [14]
Graphene-BN ( $N = \infty$ )	135	108 [14]	–
MoS <sub>2</sub> -BN ( $N = \infty$ )	26.7	20 [14]	–

Table II. Comparison of TBC results at  $T = 300$  K obtained for the various  $N$ -layer 2DLM-BN interfaces using theoretical and experimental techniques.

by relating it to  $E$ , the in-plane elastic modulus of a h-BN monolayer, which quantifies the relationship between its in-plane tensile stress and axial strain. Its value, which has been measured experimentally to be 865 GPa [9], can be used to set the interlayer spring constant  $g_{\text{iso}}$  which reproduces the equivalent relationship for the cross-plane stress and strain, i.e.,  $g_{\text{iso}} = E/a = 2.54 \times 10^{21}$  N/m<sup>3</sup>, where  $a = 0.34$  nm. We may regard  $g_{\text{iso}}$  as the value for which cross-plane elastic modulus is the same as the in-plane elastic modulus or the value of  $g$  in the ‘isotropic’ limit although the stack model is not isotropic as it only describes the out-of-plane flexural motion of the h-BN layers.

Figure 5 shows the TBC of the graphene-BN and MoS<sub>2</sub>-BN interfaces at  $T = 300$  K for different values of  $g$  between 1 and 400 percent of  $g_{\text{iso}}$ . We observe that  $G_{\text{ph}}$  decreases asymptotically when  $g \gg g_{\text{iso}}$  (strong coupling regime) and  $g \ll g_{\text{iso}}$  (van der Waals regime), with  $G_{\text{ph}}$  for multilayer graphene and MoS<sub>2</sub> peaking in the  $g \sim 10^{20}$  N/m<sup>3</sup> range, an order of magnitude smaller than  $g_{\text{iso}}$ . This peak position can be estimated by comparing the cross-plane acoustic impedance of the 2DLM, given by  $z_0 = \sqrt{\rho g_{2D}}$  where  $g_{2D}$  is the interlayer spring constant in graphene or MoS<sub>2</sub>, with the cross-plane acoustic impedance of h-BN. Given that  $z_0 = 9.14 \times 10^6$  and  $1.62 \times 10^7$  Pa·s/m for graphene and MoS<sub>2</sub>, respectively, the interlayer spring constant in h-BN has to be around  $g = z_0^2/\rho_{\text{BN}} \sim 10^{20}$  N/m<sup>3</sup>, where  $\rho_{\text{BN}}$  is the areal mass density of the h-BN monolayer, in order for the acoustic impedance of h-BN to match that of the 2DLM to maximize cross-plane transmission.

### C. Interfacial phonon transmission spectra

To understand the trends in Fig. 3, we plot the transmission spectra  $\xi(\omega)$  from Eq. (2) for  $N = 1, 5, \infty$  layers and  $T = 300$  K. The increase in  $G_{\text{ph}}$  with  $N$  can be explained by the growth of the low-frequency transmission spectra as  $N$  increases, which permits more phonon transmission across the 2DLM-substrate interface. The higher TBC for the graphene-SiO<sub>2</sub> interface relative to the graphene-BN interface in single and few-layer graphene can be explained by its larger transmission spectra  $\xi(\omega)$  at higher frequencies, as shown in Fig. 6(a) where the graphene-SiO<sub>2</sub> spectra are larger at higher fre-

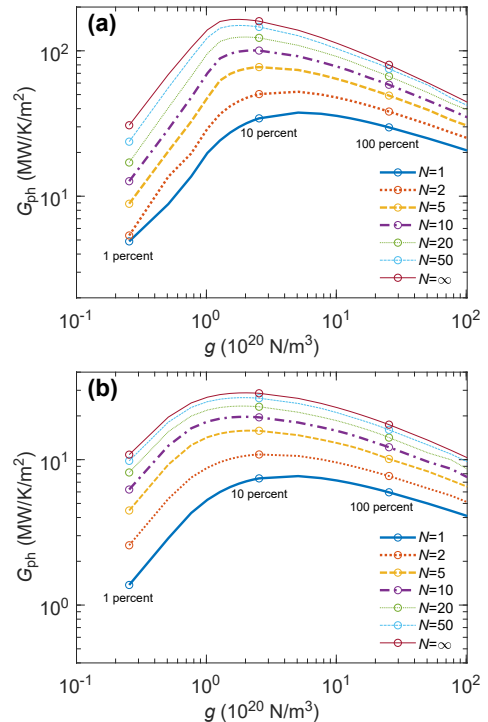


Figure 5. Plot of the TBC  $G_{\text{ph}}$  at  $T = 300$  K for  $N$ -layer (a) graphene and (b) MoS<sub>2</sub> with h-BN as the substrate for different values of  $g$ , the interlayer spring constant in h-BN. The TBC is shown for  $N = 1, 2, 5, 10, 20, 50$  and  $\infty$ . We vary the value of  $g$  from 1 to 400 percent of  $g_{\text{iso}}$  where  $g_{\text{iso}} = 2.54 \times 10^{21}$  N/m<sup>3</sup>.

quencies ( $\omega \gtrsim 20$  meV) but smaller at lower frequencies ( $\omega < 20$  meV) than the graphene-BN transmission spectra with the relative difference between the two spectra narrowing as  $N$  increases.

Figure 6(b) shows the corresponding transmission spectra for the MoS<sub>2</sub>-SiO<sub>2</sub> and MoS<sub>2</sub>-BN interfaces at  $T = 300$  K. At high frequencies ( $\omega > 19$  meV),  $\xi(\omega)$  is greater for the MoS<sub>2</sub>-SiO<sub>2</sub> interface than that for the MoS<sub>2</sub>-BN interface at  $N = 1, 5$  and  $\infty$ . On the other hand in the low-frequency regime ( $\omega < 19$  meV),  $\xi(\omega)$  is considerably greater for the MoS<sub>2</sub>-BN interface, indicating that h-BN is much more transparent to low-frequency phonon transmission from MoS<sub>2</sub> than SiO<sub>2</sub> is. This explains the substantially larger TBC of the MoS<sub>2</sub>-BN in-



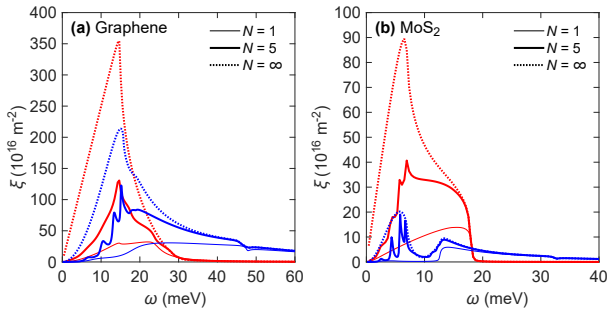


Figure 6. Plot of the interfacial transmission spectrum  $\xi(\omega)$  for (a) graphene and (b) MoS<sub>2</sub> with a-SiO<sub>2</sub> (blue lines) or h-BN (red lines) as the substrate at  $T = 300$  K for  $N = 1$  (thin solid lines), 5 (thick solid lines) and  $\infty$  (dotted lines).

terface compared to the MoS<sub>2</sub>-SiO<sub>2</sub> interface.

#### D. Comparison with the Atomistic Green's Function model

In Fig. 7, we compare the results for the transmission spectra  $\xi(\omega)$  and the TBC  $G_{\text{ph}}$  from our stack model with the more detailed ones from the AGF model [43], which treats the interfacial thermal transport between two semi-infinite ( $N = \infty$ ) crystal lattices, for the graphite-BN (i.e. graphene-BN for  $N = \infty$ ) and molybdenite-BN (i.e. MoS<sub>2</sub>-BN for  $N = \infty$ ) interface. The AGF spectra are taken from Ref. [14]. In our AGF simulation, the individual graphene layers are stacked in the A-B configuration while the individual h-BN and MoS<sub>2</sub> layers are stacked in the A-A' configuration. The cross-sectional area of the 2DLM interface is  $2.49 \times 2.16$  nm<sup>2</sup>. We note here that the following TBC results are obtained from a purely elastic treatment.

Figure 7(a) shows the  $\xi(\omega)$  for the graphene-BN interface calculated with the stack and AGF model. Unlike the  $\xi(\omega)$  of the stack model which varies smoothly with  $\omega$ , the  $\xi(\omega)$  of the AGF model has discrete steps due to the relatively small finite size of the interfacial cross section in the AGF simulation [14], which limits the number of modes contributing to the thermal conductance. In spite of the approximations used in our stack model, its  $\xi(\omega)$  shows remarkably good qualitative and even close quantitative agreement with the  $\xi(\omega)$  of the AGF model, especially in the  $\omega < 20$  meV frequency range. At higher frequencies, the transmission spectra diverge from one another because the flexural phonon dispersion in graphene becomes non-parabolic away from the Brillouin zone center. Nevertheless, this close agreement between the AGF model and our stack model, which contains only flexural modes, validates the assumptions used in the stack model and suggests that heat conduction across the graphene-BN interface is dominated by the coupling of flexural phonons between graphene and h-BN, with the in-plane

acoustic and optical phonons playing an insignificant role.

Likewise in Fig. 7(b), we also observe close agreement between the MoS<sub>2</sub>-BN transmission spectra of the the stack and AGF models in the  $\omega < 7.4$  meV frequency range, indicating the similarly dominant role of the flexural phonon coupling in interfacial heat conduction. Above this frequency range, the difference in  $\xi(\omega)$  becomes significant and we observe transmission peaks in the  $\xi(\omega)$  of the AGF model, which we attribute to the possible coupling to other acoustic and optical phonon modes because of the greater number of degrees of freedom in the MoS<sub>2</sub> unit cell.

We compare the corresponding temperature-dependent TBC from Eq. (1) for the graphene-BN interface in Fig. 7(c) which shows relatively good agreement between the stack and the AGF model especially at low temperatures ( $T \lesssim 40$  K). At  $T = 300$  K, we obtain  $G_{\text{ph}} = 135$  MW/K/m<sup>2</sup> and 108 MW/K/m<sup>2</sup> for the stack and AGF model, respectively, i.e., the stack model overpredicts the TBC. The higher  $G_{\text{ph}}$  for the stack model is due to its additional transmission contribution in  $\xi(\omega)$  for  $\omega > 20$  meV. For the MoS<sub>2</sub>-BN interface in Fig. 7(d), we have  $G_{\text{ph}} = 27$  MW/K/m<sup>2</sup> and 20 MW/K/m<sup>2</sup> for the stack model and AGF method, respectively, at  $T = 300$  K with the two  $G_{\text{ph}}$  curves converging at low temperatures ( $T \lesssim 20$  K). At higher temperatures, the difference in the  $G_{\text{ph}}$  is due to the larger  $\xi(\omega)$  in the stack model for  $\omega > 7.4$  meV. Nonetheless, the relative closeness of the  $G_{\text{ph}}$  between the stack and AGF model supports and validates the description of the elastic properties of the h-BN layers using Eqs. (5) and (6).

#### IV. SUMMARY AND CONCLUSION

To understand the limits of heat dissipation from an  $N$ -layer 2DLM (e.g. graphene or MoS<sub>2</sub>) to its h-BN substrate, we have developed a theory that depends on the elastic parameters of the 2DLM, h-BN and their interface. In our theory, we use a stack model of the h-BN substrate, in which the crystal is treated as a semi-infinite stack of harmonically coupled thin plates to describe its surface flexural response function  $D_{\text{sub}}(\mathbf{q}, \omega)$  to an external force, to determine the TBC. We find that the TBC of the interface between the 2DLM and h-BN increases with  $N$ , as with the case for an isotropic solid substrate such as a-SiO<sub>2</sub>. The increase of the TBC with  $N$  is stronger for h-BN than for a-SiO<sub>2</sub> especially when the 2DLM is MoS<sub>2</sub>. Our analysis shows that h-BN is more transparent to low-frequency phonon transmission from the 2DLM (graphene and MoS<sub>2</sub>) than a-SiO<sub>2</sub> is. At large  $N$ , h-BN is a considerably more effective substrate for heat dissipation from MoS<sub>2</sub> than a-SiO<sub>2</sub> is because of the much greater low-frequency phonon transmission. We also compare the predictions of the stack model in

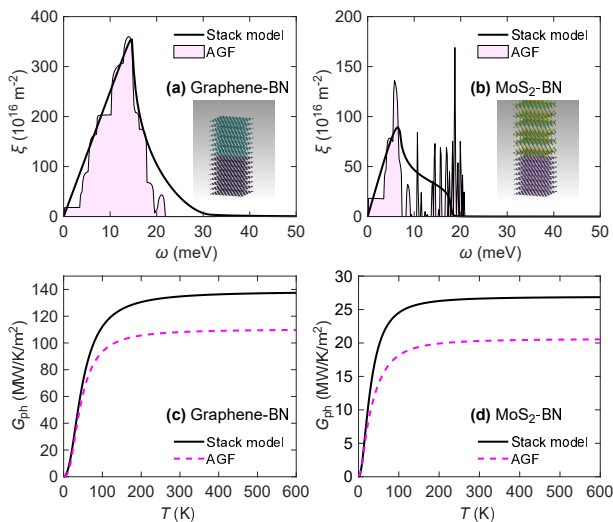


Figure 7. Comparison of the interfacial transmission spectra  $\xi(\omega)$  for the (a) graphene-BN and (b) MoS<sub>2</sub>-BN interface computed with the stack and AGF models for  $N = \infty$ . The inset in each panel shows the atomistic structure of the 2DLM-BN interface. The corresponding temperature-dependent TBC  $G_{\text{ph}}$  from  $T = 1$  to 600 K for the (c) graphene-BN and (d) MoS<sub>2</sub>-BN interface are also shown.

the  $N = \infty$  limit for the graphene-BN and MoS<sub>2</sub>-BN interface to those of the AGF model. The good agreement in the low-frequency phonon transmission spectra of the two models validates our assumption that the out-of-plane flexural modes play a key role in interfacial thermal transport. Our stack model provides clear insights into how heat dissipation from the 2DLM is affected by the anisotropy and elastic properties of a layered substrate like h-BN.

We gratefully acknowledge support from the Science and Engineering Research Council through grant (152-70-00017) and use of computing resources at the A\*STAR Computational Resource Centre and National Supercomputer Centre, Singapore.

\* ongzy@ihpc.a-star.edu.sg

[1] C. R. Dean, A. F. Young, I. Meric, C. Lee, L. Wang, S. Sorgenfrei, K. Watanabe, T. Taniguchi, P. Kim, K. L. Shepard, and J. Hone, *Nature Nanotechnology* **5**, 722 (2010), arXiv:1005.4917.  
 [2] G. H. Lee, Y. J. Yu, X. Cui, N. Petrone, C. H. Lee, M. S. Choi, D. Y. Lee, C. Lee, W. J. Yoo, K. Watanabe, T. Taniguchi, C. Nuckolls, P. Kim, and J. Hone, *ACS Nano* **7**, 7931 (2013).  
 [3] W. G. Cullen, M. Yamamoto, K. M. Burson, J. H. Chen, C. Jang, L. Li, M. S. Fuhrer, and E. D. Williams, *Phys. Rev. Lett.* **105**, 215504 (2010).  
 [4] E. Paek and G. S. Hwang, *J. Appl. Phys.* **113** (2013), 10.1063/1.4801880.

[5] Z.-Y. Ong, B. Qiu, S. Xu, X. Ruan, and E. Pop, *J. Appl. Phys.* **123**, 115107 (2018).  
 [6] J. Guo, F. Yang, M. Xia, X. Xu, and B. Li, *J. Phys. D: Appl. Phys.* **52**, 385306 (2019).  
 [7] L. Lindsay and D. A. Broido, *Phys. Rev. B* **84**, 155421 (2011).  
 [8] L. H. Li and Y. Chen, *Advanced Functional Materials* **26**, 2594 (2016).  
 [9] A. Falin, Q. Cai, E. J. Santos, D. Scullion, D. Qian, R. Zhang, Z. Yang, S. Huang, K. Watanabe, T. Taniguchi, M. R. Barnett, Y. Chen, R. S. Ruoff, and L. H. Li, *Nature Communications* **8**, 15815 (2017).  
 [10] J. Wang, F. Ma, and M. Sun, *RSC Advances* **7**, 16801 (2017).  
 [11] E. Pop, *Nano Research* **3**, 147 (2010).  
 [12] Z.-Y. Ong and M.-H. Bae, *2D Materials* **6**, 32005 (2019).  
 [13] D. Rhodes, S. H. Chae, R. Ribeiro-Palau, and J. Hone, *Nature Materials* **18**, 541 (2019).  
 [14] Y. Liu, Z.-Y. Ong, J. Wu, Y. Zhao, K. Watanabe, T. Taniguchi, D. Chi, G. Zhang, J. T. Thong, C. W. Qiu, and K. Hippalgaonkar, *Scientific Reports* **7**, 43886 (2017).  
 [15] S. Vaziri, E. Yalon, M. M. Rojo, S. V. Suryavanshi, H. Zhang, C. J. McClellan, C. S. Bailey, K. K. Smithe, A. J. Gabourie, V. Chen, S. Deshmukh, L. Bendersky, A. V. Davydov, and E. Pop, *Science Advances* **5**, eaax1325 (2019).  
 [16] B. N. J. Persson, A. I. Volokitin, and H. Ueba, *J. Phys.: Condens. Matter* **23**, 45009 (2011).  
 [17] Z.-Y. Ong, Y. Cai, and G. Zhang, *Phys. Rev. B* **94**, 165427 (2016).  
 [18] Z.-Y. Ong, *Phys. Rev. B* **95**, 155309 (2017).  
 [19] B. N. Persson, *J. Chem. Phys.* **115**, 3840 (2001).  
 [20] Y. Zhao, X. Luo, H. Li, J. Zhang, P. T. Araujo, C. K. Gan, J. Wu, H. Zhang, S. Y. Quek, M. S. Dresselhaus, and Q. Xiong, *Nano Lett.* **13**, 1007 (2013).  
 [21] L. Liang, J. Zhang, B. G. Sumpter, Q. H. Tan, P. H. Tan, and V. Meunier, *ACS Nano* **11**, 11777 (2017).  
 [22] B. Amorim and F. Guinea, *Phys. Rev. B* **88**, 115418 (2013), arXiv:1304.6567.  
 [23] C. A. Polanco and L. Lindsay, *Phys. Rev. B* **97**, 14303 (2018).  
 [24] Y. Wei and R. Yang, *National Science Review* **6**, 324 (2019).  
 [25] S. Li and Y. Chen, *Scientific Reports* **7**, 43956 (2017).  
 [26] N. Bonini, J. Garg, and N. Marzari, *Nano Letters* **12**, 2673 (2012).  
 [27] G. Chen, *Nanoscale energy transport and conversion: a parallel treatment of electrons, molecules, phonons, and photons* (Oxford University Press, New York, 2005).  
 [28] L. Lindsay, W. Li, J. Carrete, N. Mingo, D. A. Broido, and T. L. Reinecke, *Phys. Rev. B* **89**, 155426 (2014).  
 [29] S. Sadasivam, N. Ye, J. P. Feser, J. Charles, K. Miao, T. Kubis, and T. S. Fisher, *Phys. Rev. B* **95**, 085310 (2017), arXiv:1609.03063.  
 [30] S. K. Singh, M. Neek-Amal, S. Costamagna, and F. M. Peeters, *Phys. Rev. B* **87**, 184106 (2013), arXiv:1304.5972.  
 [31] K. E. Goodson, M. I. Flik, L. T. Su, and D. A. Antoniadis, *J. Heat Transfer* **116**, 317 (1994).  
 [32] P. E. Hopkins, J. C. Duda, and P. M. Norris, *J. Heat Transfer* **133**, 62401 (2011).  
 [33] N. Mingo, *Phys. Rev. B* **74**, 125402 (2006).  
 [34] J. Dai and Z. Tian, *Phys. Rev. B* **101**, 041301(R) (2020).

- [35] J. T. Gaskins, G. Kotsonis, A. Giri, S. Ju, A. Rohskopf, Y. Wang, T. Bai, E. Sachet, C. T. Shelton, Z. Liu, Z. Cheng, B. M. Foley, S. Graham, T. Luo, A. Henry, M. S. Goorsky, J. Shiomi, J. P. Maria, and P. E. Hopkins, *Nano Lett.* **18**, 7469 (2018).
- [36] Z. Cheng, Y. R. Koh, H. Ahmad, R. Hu, J. Shi, M. E. Liao, Y. Wang, T. Bai, R. Li, E. Lee, E. A. Clinton, C. M. Matthews, Z. Engel, L. Yates, T. Luo, M. S. Goorsky, W. A. Doolittle, Z. Tian, P. E. Hopkins, and S. Graham, *Communications Physics* **3**, 115 (2020).
- [37] D. G. Cahill and R. O. Pohl, *Annual Review of Physical Chemistry* **39**, 93 (1988).
- [38] S. M. Lee and D. G. Cahill, *J. Appl. Phys.* **81**, 2590 (1997).
- [39] T. Yamane, N. Nagai, S. I. Katayama, and M. Todoki, *J. Appl. Phys.* **91**, 9772 (2002).
- [40] J. M. Larkin and A. J. H. McGaughey, *Phys. Rev. B* **89**, 144303 (2014).
- [41] C. C. Chen, Z. Li, L. Shi, and S. B. Cronin, *Appl. Phys. Lett.* **104**, 081908 (2014).
- [42] D. Kim, H. Kim, W. S. Yun, K. Watanabe, T. Taniguchi, H. Rho, and M. H. Bae, *2D Materials* **5**, 025009 (2018).
- [43] W. Zhang, T. S. Fisher, and N. Mingo, *Numer. Heat Transfer, Part B* **51**, 333 (2007).